

1 **Organic amine weakens chloride depletion in coastal**  
2 **atmosphere**

3 Aijing Song<sup>1</sup>, Kun Li<sup>1</sup>, Zhaomin Yang<sup>1</sup>, Li Xu<sup>2</sup>, Narcisse Tsona Tchinda<sup>1</sup>, and Lin  
4 Du<sup>1,2,3,\*</sup>

5 <sup>1</sup>Qingdao Key Laboratory for Prevention and Control of Atmospheric Pollution in Coastal Cities,  
6 Environment Research Institute, Shandong University, Qingdao 266237, China

7 <sup>2</sup>School of Environmental Science and Engineering, Shandong University, Qingdao 266237, China

8 <sup>3</sup>State Key Laboratory of Microbial Technology, Shandong University, Qingdao 266237, China

9 *Correspondence to: Lin Du (lindu@sdu.edu.cn)*

10 \_\_\_\_\_

11 **Abstract.** Chloride depletion from sea salt aerosols (SSA) is frequently observed in polluted coastal  
12 regions, and despite they severely impact air quality and human health, the influencing mechanism of  
13 alkaline species in this phenomenon remains incompletely understood. Here, we conducted laboratory  
14 experiments to investigate the effect of alkaline species including  $\text{NH}_3$  and an organic amine  
15 (dimethylamine, DMA) on chloride depletion and the subsequent formation of organic chlorinated  
16 compounds. Results showed that alkaline species could weaken chloride depletion caused by acidic  
17 gases, mainly due to acid-base neutralization. Specifically, chloride depletion in the presence of  $\text{NO}_x$   
18 decreased from 20.1% to 15.8% when  $\text{NH}_3$  concentration increased from 100 to 300 ppb. Chloride  
19 depletion also decreased from 18.6% to 13.5% with DMA concentration increasing from 50 to 150 ppb.  
20 The weakening effect of DMA on chloride depletion is more pronounced than that of  $\text{NH}_3$ , primarily  
21 DMA stronger alkalinity and nucleation ability. These alkaline species exhibit a stronger reduction of  
22 chloride depletion in the presence of  $\text{SO}_2$  than in the presence of  $\text{NO}_x$ . The detection of organic  
23 chlorinated products, formed via active chlorine-induced oxidation, is consistent with the role of  
24 alkaline species in weakening chloride depletion, which subsequently results in the reduction of active  
25 chlorine. These findings suggest that alkaline species, more specifically organic amines, are significant  
26 factors influencing chloride depletion in the coastal atmosphere, further improving our understanding  
27 of this phenomenon.

## 28 **1 Introduction**

29 Sea salt aerosols (SSA), primarily composed of sodium chloride, are abundant in coastal areas and play  
30 a key role in cloud nucleation with high light scattering efficiency (Zhang and Chan, 2023; Zhou et al.,  
31 2025). Chloride depletion, referred to as the removal of chloride ions from SSA and frequently  
32 observed in the coastal atmosphere (Bian et al., 2014; Duan et al., 2024; Su et al., 2022), accelerates  
33 their aging process of SSA, profoundly influencing visibility, global climate and the earth-atmosphere  
34 radiative balance (Ghosh et al., 2020; Edwards et al., 2024; Su et al., 2022). This process also affects  
35 the atmospheric oxidation capacity by producing  $\text{Cl}_2$ ,  $\text{HCl}$ ,  $\text{Cl}^\bullet$ , and other reactive species (Hoffmann et  
36 al., 2019; Chen et al., 2024b; Dai et al., 2025). However, significant discrepancies exist between field  
37 observations and model predictions of chloride depletion with an average absolute difference of 20%  
38 (Nolte et al., 2008; Nolte et al., 2015; Su et al., 2022), highlighting the need for a deeper understanding

39 of its underlying mechanisms.

40 Alkaline species such as  $\text{NH}_3$  and organic amines have been suspected to affect chloride depletion (Su  
41 et al., 2022). Gaseous ammonia ( $\text{NH}_3$ ), the most abundant alkaline species in the atmosphere, plays an  
42 important role in the formation of atmospheric particles (Behera et al., 2013; Lan et al., 2024; Wang et  
43 al., 2020). A field study found a relatively low level of chloride depletion in the Antarctic winter, and  
44 the large amount of ammonia emitted by penguins has been hypothesized to be responsible for this  
45 phenomenon (Rankin and Wolff, 2003). Dimethylamine (DMA,  $(\text{CH}_3)_2\text{NH}$ ), a predominant organic  
46 amine in the atmosphere, has a stronger alkalinity than ammonia and could compete with ammonia in  
47 reactions with acidic species, despite its atmospheric concentration being much lower than that of  
48 ammonia (Chen et al., 2022; Xie et al., 2018; Liu et al., 2024a). However, to the best of our knowledge,  
49 there is currently no experimental evidence illustrating the role of alkaline species in chloride depletion.

50 The influence of organic amines remains overlooked in model predictions (Nolte et al., 2015),  
51 highlighting a critical gap for accurately predicting chloride depletion in amine-rich coastal or  
52 agricultural-marine interfaces.

53 Organic chlorinated compounds are important indicators of chloride depletion. They can be formed  
54 from the oxidation of volatile organic compounds (VOCs) by reactive chlorine species (e.g.,  $\text{Cl}^\bullet$ ,  $\text{Cl}_2^\bullet$ ,  
55 etc.) generated during the chloride depletion process (Zhang and Chan, 2023; Wennberg et al., 2018;  
56 Wang et al., 2022b). Once formed, some organic chlorinated compounds with low volatility can  
57 partition into the particle phase, contributing to the formation of secondary organic aerosols (SOA). For  
58 example, it is estimated that organic chlorinated compounds can contribute up to 15% of the total SOA  
59 in polluted areas with sufficient chlorine and VOC emissions (Liu et al., 2024c). Organic chlorinated  
60 compounds have been observed during chloride depletion in our previous study in the presence of  
61 isoprene (Song et al., 2025), an important biogenic VOC emitted from ocean and terrestrial plants (Yu  
62 and Li, 2021; Zhang et al., 2025; Zou et al., 2023). Understanding the formation of organic chlorinated  
63 compounds would not only help elucidating the influence of alkaline species on chloride depletion but  
64 also provide significant implications for the chlorine cycle.

65 To investigate the roles of alkaline species, including  $\text{NH}_3$  and DMA, in chloride depletion,  
66 experiments on reactions involving SSA particles, alkaline species, acidic gases, and/or isoprene were  
67 conducted in a chamber. We characterized the changes in chloride depletion and further analyzed the  
68 subsequent formation of corresponding organic chlorinated compounds to explore the reasons for their

69 changes. This study provides a comprehensive understanding of chloride depletion from SSA, which  
70 may be crucial for more accurately predicting this phenomenon in coastal atmospheres.

## 71 2 Materials and methods

### 72 2.1 Chamber experiments

73 To study the effect of alkaline species on chloride depletion, three groups of experiments were designed:  
74 NaCl particles + NH<sub>3</sub>/DMA (control experiments), NaCl particles + H<sub>2</sub>O<sub>2</sub> + NO<sub>x</sub>/SO<sub>2</sub> + NH<sub>3</sub>/DMA,  
75 and NaCl particles + H<sub>2</sub>O<sub>2</sub> + isoprene + NO<sub>x</sub>/SO<sub>2</sub> + NH<sub>3</sub>/DMA. Here, the shifting ratios of ammonia to  
76 DMA are in the range 0.67-6, which falls within the ranges observed in diverse coastal environments  
77 (0.1-110) (Smith et al., 2007; Chen et al., 2022; Berner and David Felix, 2020; Liu et al., 2022; Liu et  
78 al., 2024b; Liu et al., 2023; Du et al., 2021). Although the initial concentrations of alkaline species used  
79 in the experiments were higher than the ambient levels, this consideration was necessary for laboratory  
80 experiments within a short time scale to tackle their influence on chloride depletion. Details of  
81 experimental conditions are provided in Table 1. All experiments were conducted in a 1.5 m<sup>3</sup> indoor  
82 chamber consisting of 60 μm Teflon film within a temperature-controlled environment, surrounded by  
83 black light lamps (F40BLB, GE) with the center irradiation wavelength of 365 nm as the light source.  
84 The chamber was equipped with a set of online instruments for measuring physical and chemical  
85 parameters. The concentration of aerosol particles was measured using a scanning mobility particle  
86 sizer (SMPS, Grimm, Germany), which is composed of a differential mobility analyzer (DMA, 55-L,  
87 Grimm, Germany) and a condensation particle counter (CPC, 5416, Grimm, Germany). The  
88 concentrations of NO<sub>x</sub> and isoprene in the chamber were monitored using a NO–NO<sub>2</sub>–NO<sub>x</sub> analyzer  
89 (Model 42i, Thermo Scientific, USA) and a gas chromatograph coupled with a flame ionization  
90 detector (GC-FID 7890B, Agilent Technologies, USA). H<sub>2</sub>O<sub>2</sub> acted as the source of OH radicals. The  
91 initial concentrations of other substances (H<sub>2</sub>O<sub>2</sub>, alkaline gases, etc.) were calculated based on the  
92 chamber volume and the injection volume.

93 **Table 1. Summary of experimental conditions and results.**

Experiment <sup>a</sup>	[Isoprene] <sub>0</sub>	[H <sub>2</sub> O <sub>2</sub> ] <sub>0</sub>	[NO <sub>x</sub> ] <sub>0</sub>	[SO <sub>2</sub> ] <sub>0</sub>	[NH <sub>3</sub> ] <sub>0</sub>	[DMA] <sub>0</sub>	RH	T	Cl <sup>-</sup> /Na <sup>+</sup>
	(ppb)	(ppm)	(ppb)	(ppb)	(ppb)	(ppb)	(%)	(°C)	(mM/mM) <sup>c</sup>
C.1					100		72	20	0.989±0.019

C.2				100	71	20	0.994±0.020
N.1		4	141		69	23	0.755±0.015
NA.1		4	138	100	69	21	0.798±0.016
NA.2		4	139	200	72	21	0.822±0.017
NA.3		4	139	300	72	20	0.841±0.017
ND.1		4	146	50	69	21	0.813±0.017
ND.2		4	147	100	71	21	0.849±0.017
ND.3		4	141	150	71	22	0.864±0.018
S.1		4	300		67	22	0.704±0.009
SA.1		4	300	100	70	23	0.825±0.017
SA.2		4	300	200	70	23	0.839±0.017
SA.3		4	300	300	69	23	0.849±0.017
SD.1		4	300	50	70	22	0.851±0.017
SD.2		4	300	100	71	22	0.865±0.018
SD.3		4	300	150	70	23	0.878±0.018
IN.1 <sup>b</sup>	667	4	150		72	20	0.770±0.016
INA.1 <sup>b</sup>	621	4	140	100	71	22	0.784±0.016
INA.2	604	4	161	300	69	23	0.791±0.016
IND.1 <sup>b</sup>	601	4	152	100	68	22	0.814±0.017
IND.2	668	4	146	150	70	20	0.866±0.018
IS.1 <sup>b</sup>	776	4	300		68	20	0.655±0.008
ISA.1 <sup>b</sup>	604	4	300	100	70	20	0.790±0.016
ISA.2	601	4	300	300	71	21	0.800±0.016
ISD.1 <sup>b</sup>	629	4	300	100	70	21	0.897±0.018
ISD.2	594	4	300	150	69	22	0.961±0.020

94 <sup>a</sup>Abbreviations used in experimental codes correspond to the reactants introduced into the chamber.  
95 “N”, “S”, “A”, “D”, and “I” stand for NO<sub>x</sub>, SO<sub>2</sub>, NH<sub>3</sub>, DMA, and isoprene, respectively. C.1 and C.2  
96 are control experiments.  
97 <sup>b</sup>Experiments were repeated to collect aerosol particles for composition measurement by  
98 UPLC/ESI-HR-Q-TOFMS.  
99 <sup>c</sup>Errors in Cl<sup>-</sup>/Na<sup>+</sup> were calculated by error propagation considering Cl<sup>-</sup> and Na<sup>+</sup> errors derived from  
100 their IC calibration curve.

101 The chamber was thoroughly cleaned using O<sub>3</sub> and purified air, and exposed to UV lamps for at least  
102 12 h before each experiment. Relative humidity (RH) in the chamber was adjusted by the proportion of  
103 dry and wet air. Subsequently, SSA particles produced by atomizing NaCl solution with an atomizer  
104 (Model 3076, TSI, USA) were introduced into the chamber. Based on the experimental design, known  
105 volumes of other reactants (i.e., H<sub>2</sub>O<sub>2</sub> (Aladdin, 30 wt% in H<sub>2</sub>O), inorganic gases (NH<sub>3</sub>, NO, etc)  
106 (Qingdao Deyi Gas Company, 500 ppm balanced in N<sub>2</sub>), DMA (Aladdin, 40 wt% in H<sub>2</sub>O), and isoprene  
107 (Macklin, >99%)) were introduced into the chamber. After the reactants were adequately mixed for 20  
108 minutes, the black light lamps were turned on to initiate the reaction. The experiment lasted for two  
109 hours, after which aerosol particles generated during the experiment were collected onto quartz filters  
110 and 47 mm polytetrafluoroethylene (PTFE) filters and stored at -20 °C until offline analysis.

## 111 **2.2 Particle analysis**

112 The concentrations of inorganic ions were measured by ion chromatography (IC, Dionex ICS-600,  
113 Thermo Scientific, USA). Aerosol particles collected on the quartz filters were first extracted in 5 mL  
114 of ultrapure water (Milli-Q, Millipore, France) by ice sonication for 45 min. The extract was then  
115 filtered through a 0.22 μm polyethersulfone syringe filter and injected into the ion chromatography  
116 instrument via a six-way valve with a 250-μL loop. The separation of anions and cations was achieved  
117 using a Dionex IonPac AS19 column (4 × 250 mm) with an AG19 guard column (4 × 50 mm, Dionex  
118 Ionpac) for anions, and a Dionex IonPac CS12A column (4 × 250 mm) with a CG12A guard column (4  
119 × 50 mm, Dionex Ionpac) for cations. A 20 mM potassium hydroxide solution was used as the anionic  
120 eluent, while a 20 mM methanesulfonic acid solution was employed for cationic elution. The flow rate  
121 for both eluents was maintained at 1 mL min<sup>-1</sup>. The degree of chloride depletion was characterized by  
122 the mole ratios of Cl<sup>-</sup>/Na<sup>+</sup>. The Cl<sup>-</sup>/Na<sup>+</sup> value for fresh SSA is around 0.999, while lower Cl<sup>-</sup>/Na<sup>+</sup> ratios  
123 in SSA indicate the occurrence of chloride depletion.

124 The formation of organic chlorinated compounds was characterized using ultra-high performance  
125 liquid chromatography (UPLC, UltiMate 3000, Thermo Scientific, USA) coupled with electrospray  
126 ionization high-resolution quadrupole time-of-flight mass spectrometer (ESI-HR-Q-TOF-MS, Bruker  
127 Impact HD, Germany). Prior to measurements, aerosol particles collected on PTFE filters were  
128 extracted twice using 5 mL methanol (Optima® LC/MS grade, Fisher Scientific, USA) by sonication in  
129 an ice bath for 30 min. The extract was filtered through a PTFE syringe filter (0.22 μm) to remove

130 impurities, and then concentrated under a gentle nitrogen gas (99.999%, Qingdao Deyi Gas Company).  
131 The dried extract was reconstituted in 200  $\mu\text{L}$  of a 1:1 (v:v) mixture of methanol and ultrapure water  
132 containing 0.1% formic acid (Optima® LC/MS grade, Fisher Scientific, USA). Sample extracts (10  $\mu\text{L}$ )  
133 were analyzed using an Atlantis T3 C18 column (100  $\text{\AA}$ , 3  $\mu\text{m}$  particle size, 2.1 mm  $\times$  150 mm, Waters,  
134 USA). The mobile phase comprised 0.1% formic acid in ultrapure water (A) and 0.1% formic acid in  
135 methanol (B). A 60 min gradient elution with a flow of 200  $\mu\text{L min}^{-1}$  was performed as follows: B  
136 initially maintained at 3% for the first 3 minutes, gradually increased to 50% from 3 to 25 minutes, and  
137 then rose to 90% from 25 to 43 minutes. The fraction of B was reduced back to 3% between 43 and 48  
138 minutes, and maintained at 3% until 60 minutes to re-equilibrate the column.

139 Mass spectrometric data were analyzed with Bruker Compass Data Analysis version 4.2 Build 383.1  
140 software. The molecular formulas of organic chlorinated compounds were assigned as  
141  $\text{C}_{2-40}\text{H}_{2-80}\text{O}_{0-40}\text{N}_{0-3}\text{S}_{0-2}\text{Cl}_{1-2}$  within a  $\pm 5$  ppm mass tolerance, with restrictive conditions applied to  
142 exclude unreasonable formulas:  $1 \leq \text{H/C} \leq 3$ ,  $0.2 \leq \text{O/C} < 1.5$ ,  $0 \leq \text{N/C} \leq 0.5$ ,  $0 \leq \text{S/C} \leq 1$ ,  $\text{S/O} \leq 0.25$ ,  $0$   
143  $<$  double bond equivalent (DBE)/C  $< 1$ . The organic chlorinated compounds were reliably identified  
144 based on their isotopic mass and intensity, but the identified formulas containing isotopes (e.g.,  $^{13}\text{C}$ ,  $^{18}\text{O}$ ,  
145  $^{34}\text{S}$ , and  $^{37}\text{Cl}$ ) were not further discussed. The carbon oxidation state ( $\text{OS}_\text{C}$ ) and DBE of the assigned  
146 molecular formula ( $\text{C}_c\text{H}_h\text{O}_o\text{N}_n\text{S}_s\text{Cl}_j$ ) were calculated as follows:

$$147 \quad \text{DBE} = 1 + \frac{2c - (h+j) + n}{2} \quad (1)$$

$$148 \quad \text{OS}_\text{C} \approx 2 \times \frac{\text{O}}{\text{C}} - \frac{\text{H}}{\text{C}} \quad (2)$$

149 The toxicity of identified organic chlorinated compounds was analyzed based on their possible  
150 chemical structures using Toxicity Estimation Software Tool (T.E.S.T., V.5.1.2, USEPA) to estimate  
151 their oral rat  $\text{pLD}_{50}$  ( $-\log_{10}(\text{pred})$ ,  $\text{mol kg}^{-1}$ ), developmental toxicity, and mutagenicity.

### 152 **2.3 Box model**

153 The Framework for 0-D Atmospheric Modeling (F0AM) (Wolfe et al., 2016) was used to further  
154 investigate the impact of alkaline species on chloride depletion. The gas phase reactions used in this  
155 study were derived from the Master Chemical Mechanism (MCM) v3.3.1 (<http://mcm.york.ac.uk/>)  
156 (Jenkin et al., 2015). Based on the heterogeneous reactions integrated in our previous work (Song et al.,  
157 2026), we further incorporated the acid-base neutralization reactions into the mechanism, with a rate

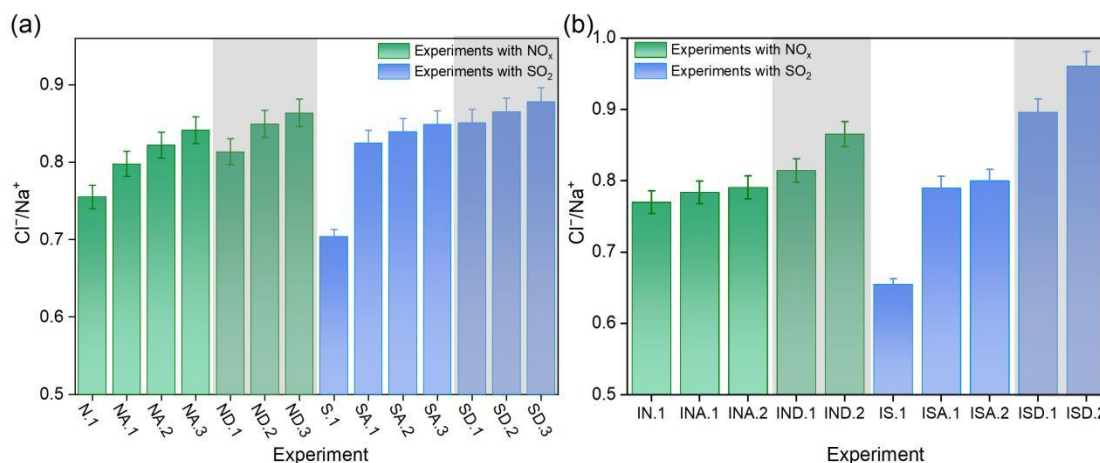
158 constant of  $2.64 \times 10^{-16} \text{ cm}^3 \text{ molecule}^{-1} \text{ s}^{-1}$  for the reaction between  $\text{NH}_3$  and  $\text{HNO}_3$  (Behera and  
159 Sharma, 2012). The initial conditions in the model were set to match those of the chamber experiments.

### 160 **3. Results and discussion**

#### 161 **3.1 Effects of $\text{NH}_3$ on chloride depletion**

162 A series of experiments were designed with varying initial concentrations of alkaline species in the  
163 presence of acid gases, i.e.,  $\text{SO}_2$  and  $\text{NO}_x$ , to evaluate the effect of alkaline species on chloride  
164 depletion (Table 1). Although  $\text{NH}_3$  addition induced no significant change in chloride depletion in the  
165 absence of  $\text{SO}_2$  and  $\text{NO}_x$  (Exp. C.1), it could significantly hinder this process in their presence (Fig. 1a).  
166 For example, the mole ratios of  $\text{Cl}^-/\text{Na}^+$  increased from 0.798 to 0.841 when the concentration of  $\text{NH}_3$   
167 raised from 100 to 300 ppb under constant  $\text{NO}_x$  (Exp.NA.1-NA.3), while this ratio was 0.755 when  
168 only  $\text{NO}_x$  was present (Exp.N.1). This corresponds to a reduction in chloride depletion from 20.1% to  
169 15.8%. In these experiments,  $\text{NO}_2 + \text{OH}$  or  $\text{N}_2\text{O}_5 + \text{H}_2\text{O}$  reactions could lead to the formation of nitric  
170 acid ( $\text{HNO}_3$ ), which can induce chloride depletion through the replacement reaction (Su et al., 2022;  
171 Xu et al., 2021). The suppressed chloride depletion by  $\text{NH}_3$  can be attributed to the neutralization  
172 reaction between  $\text{NH}_3$  and  $\text{HNO}_3$  that generates  $\text{NH}_4\text{NO}_3$  particles (Behera et al., 2013). Although  
173  $\text{NH}_4\text{NO}_3$  is unstable (Behera et al., 2013; Lan et al., 2024), ammonium ions were detected in these  
174 experiments. Furthermore, the time series of the  $\text{HNO}_3$  and Cl atoms exposure were simulated using  
175 F0AM for Exp.N.1-NA.3 (Fig. S1). The exposure of  $\text{HNO}_3$  and Cl atoms decreased after  $\text{NH}_3$  addition,  
176 further supporting the crucial role of the reaction between  $\text{NH}_3$  and  $\text{HNO}_3$  in reducing chloride  
177 depletion. As shown in Table S1, the exposure of  $\text{HNO}_3$  and Cl atoms also decreased after the addition  
178 of  $\text{NH}_3$  (0-20 ppb), demonstrating that the observed mechanisms persist at near-ambient concentrations.  
179 In the presence of  $\text{SO}_2$ , the effect of  $\text{NH}_3$  on reducing chloride depletion is even more pronounced. For  
180 example, the addition of 300 ppb  $\text{NH}_3$  (Exp.SA.3) reduced  $\text{SO}_2$ -induced chloride depletion from 29.5%  
181 (Exp.S.1) to 15.0%. This can be explained by the generation of  $(\text{NH}_4)_2\text{SO}_4$  via the reaction of  $\text{NH}_3$  with  
182 sulfuric acid ( $\text{H}_2\text{SO}_4$ ), which is produced from the oxidation of  $\text{SO}_2$  by OH radicals (Lan et al., 2024;  
183 Behera et al., 2013). As shown in Fig. S2, ammonium ion was detected in Exp.SA.1-SA.3. Notably, the  
184  $\text{H}_2\text{SO}_4 + \text{NH}_3$  reaction is much more thermodynamical and kinetically favorable than the  $\text{HNO}_3 + \text{NH}_3$   
185 reaction (Behera et al., 2013; Behera and Sharma, 2011). This may be the reason why the reduction in

186 chloride depletion was more significant in experiments SA.1-SA.3 compared to experiments  
 187 NA.1-NA.3. Our findings further support the hypothesis formulated from field studies that ammonia  
 188 can reduce chloride depletion (Rankin and Wolff, 2003; Braun et al., 2017; Zhan et al., 2017; Chen et  
 189 al., 2016; Yao et al., 2003; Ghosh et al., 2020).



190

191 **Figure 1. Dependences of Cl<sup>-</sup>/Na<sup>+</sup> ratio on the concentrations of different alkaline species in the (a) absence**  
 192 **and (b) presence of isoprene. The experiments with a grey background indicate the addition of DMA.**

193 Isoprene was further introduced into the experimental chamber with various initial NH<sub>3</sub> concentrations  
 194 to study the combined effect of alkaline gases with isoprene and acidic gases (Fig. 1b). Similar to the  
 195 above experiments without isoprene, NH<sub>3</sub> can reduce the chloride depletion caused by acidic gases,  
 196 with a more pronounced weakening effect in the presence of SO<sub>2</sub>. Notably, the addition of isoprene  
 197 reduced the ability of NH<sub>3</sub> to weaken chloride depletion, resulting in its relative enhancement. For  
 198 instance, chloride depletion was 20.8% in the experiment with isoprene and NH<sub>3</sub> (Exp.INA.2),  
 199 significantly higher than 15.8% in the experiment without isoprene (Exp.NA.3). Slightly different  
 200 values, namely 19.9% and 15.0% were observed in Exp.ISA.2 and Exp.SA.3, respectively, which can  
 201 be attributed to the reaction of NH<sub>3</sub> with SOA constituents such as organic acids, or other species  
 202 generated from the oxidation of isoprene to form nitrogen-containing organic compounds (Li et al.,  
 203 2024; Wu et al., 2021; Wennberg et al., 2018; Bates et al., 2023). This leads to reduced NH<sub>3</sub> for  
 204 neutralizing acid-induced chloride depletion.

### 205 3.2 Effects of DMA on chloride depletion

206 DMA was introduced into the reaction system to investigate its influence on chloride depletion. Similar  
 207 to NH<sub>3</sub>, DMA also caused negligible chloride depletion in the absence of acidic gases (Exp.C2, Table

208 1). In the presence of acidic gases, the weakening effect of chloride depletion becomes more  
209 pronounced with increasing DMA concentrations (Fig. 1a). For example, chloride depletion decreased  
210 from 18.6% to 13.5% as DMA concentration increased from 50 to 150 ppb in the presence of NO<sub>x</sub>  
211 (Exp.ND.1-ND.3). In the presence of SO<sub>2</sub> in Exp.SD.1-SD.3, it ranged from 12.1% to 14.8%, lower  
212 than that in Exp.S.1 (29.5%). This is mainly because DMA, with a high vapor pressure, can react with  
213 inorganic acids (e.g., HNO<sub>3</sub>, H<sub>2</sub>SO<sub>4</sub>, etc.) produced during the reaction to form aminium salts with  
214 lower vapor pressure (Wang et al., 2010; Murphy et al., 2007; Nielsen et al., 2012). Moreover, DMA  
215 can effectively promote cluster formation with H<sub>2</sub>SO<sub>4</sub> or HNO<sub>3</sub>, thereby generating DMA-H<sub>2</sub>SO<sub>4</sub>,  
216 DMA-H<sub>2</sub>SO<sub>4</sub>-H<sub>2</sub>O clusters, and other nucleation systems (Chen et al., 2024a; Loukonen et al., 2010;  
217 Zhang et al., 2019). The aforementioned mechanisms can all reduce chloride depletion induced by  
218 inorganic acids.

219 As shown in Fig. 1a, chloride depletion in Exp.ND.2 (15.0%) was lower than that in Exp.NA.1 (20.1%).  
220 Similarly, it was lower (13.4%) in Exp.SD.2 than in Exp.SA.1 (17.4%). Despite the DMA  
221 concentration is lower than that of NH<sub>3</sub>, chloride depletion in the presence of DMA (Exp.SD.1) was  
222 still weaker than that in the presence of NH<sub>3</sub> (Exp.SA.1). This can be attributed to DMA having a  
223 stronger alkalinity (Chen et al., 2022; Sauerwein and Chan, 2017; Xie et al., 2018), and a more  
224 effective nucleation ability (Ortega et al., 2012; Kupiainen et al., 2012) than NH<sub>3</sub>. According to a  
225 theoretical study by Zhang et al. (2019), DMA is more likely than NH<sub>3</sub> to approach the air-nanoparticle  
226 interface, where the probability of its heterogeneous reaction with H<sub>2</sub>SO<sub>4</sub> can increase. Notably, the  
227 neutralization efficiency of alkaline species can be affected by the particle phase state. When the phase  
228 state of particles changes from liquid to semisolid state, the neutralization efficiency of DMA may be  
229 relatively inhibited compared to that of the more mobile NH<sub>3</sub> (Sauerwein and Chan, 2017; Derieux et  
230 al., 2019). The viscosity of SSA particles in our experiments was calculated to be 1.89-1.98 Pa·s  
231 (details in the Supplement), being significantly lower than the 10<sup>2</sup> Pa·s threshold for  
232 liquid-to-semisolid phase transition (Derieux et al., 2018). This suggests that the SSA particles in this  
233 study existed in liquid state, and the neutralization efficiency of both ammonia and DMA was not  
234 constrained by phase transition.

235 Following the addition of isoprene, the weakening effect of DMA on chloride depletion in the presence  
236 of NO<sub>x</sub> was not significantly different from that of experiments without isoprene. Nonetheless, this  
237 addition enhanced the weakening effect of DMA on chloride depletion in the presence of SO<sub>2</sub>. Chloride

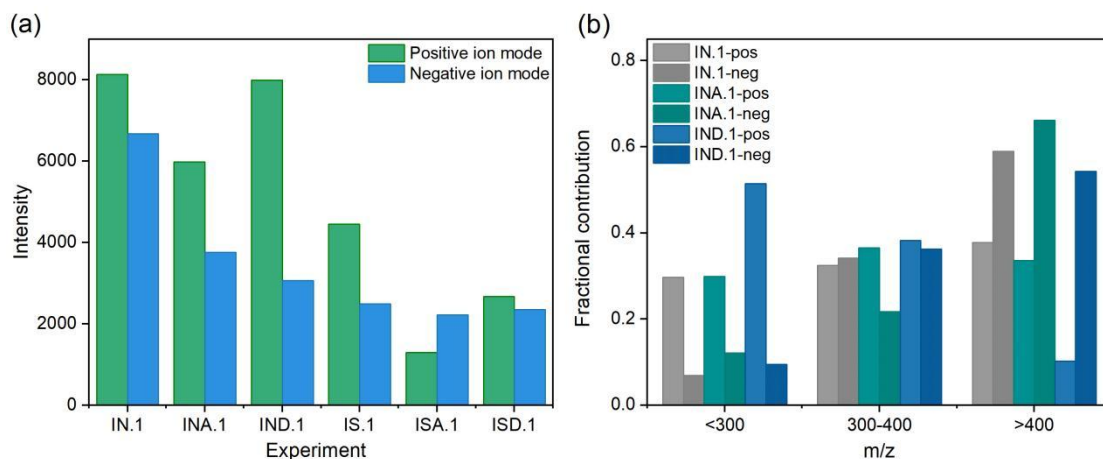
238 depletion in Exp.ISD.2 was 3.8%, significantly lower than that in Exp.SD.3 (12.1%). This can be  
239 explained by the fact that organic acids produced from the oxidation of isoprene enhance DMA-H<sub>2</sub>SO<sub>4</sub>  
240 nucleation, with a stronger enhancement effect observed at lower H<sub>2</sub>SO<sub>4</sub> concentrations (Wang et al.,  
241 2022a; Lu et al., 2020). Isoprene oxidation products can react with H<sub>2</sub>SO<sub>4</sub> to form organic sulfates  
242 (Armstrong et al., 2022; Wach et al., 2020), leading to a reduction in H<sub>2</sub>SO<sub>4</sub> concentration within the  
243 reaction system.

### 244 **3.3 Formation of organic chlorinated compounds**

245 The molecular composition of organic chlorinated compounds was analyzed, using  
246 UPLC/ESI-Q-TOF-MS, to further explore the effect of active chlorine on chloride depletion. Fig. S3  
247 presents the mass spectra of organic chlorinated compounds in the presence of acidic and alkaline gases.  
248 Mass spectra in both positive and negative ion modes contained numerous peaks, with compositions in  
249 the presence of NO<sub>x</sub> being more complex than those in the presence of SO<sub>2</sub>.

#### 250 **3.3.1 Effects of alkaline species in the presence of NO<sub>x</sub>**

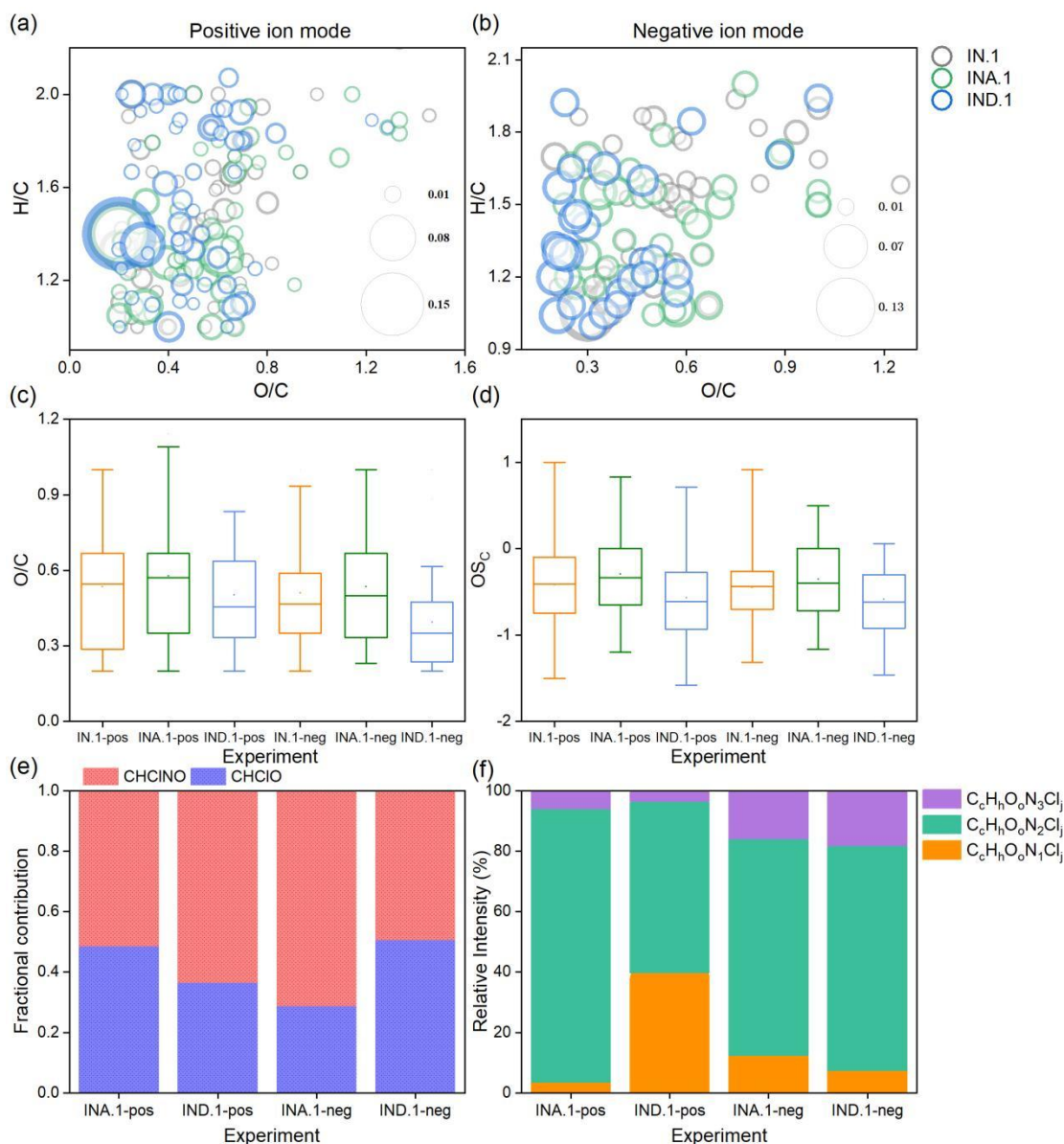
251 As shown in Fig. 2a, the total signal intensity of the organic chlorinated compounds detected in the  
252 presence of alkaline species (Exp.INA.1 and Exp.IND.1) was lower than that in their absence  
253 (Exp.IN.1), indicating that the alkaline species reduce the formation of organic chlorinated compounds  
254 during the chloride depletion process. The identified organic chlorinated compounds were classified  
255 into three categories:  $m/z < 300$ ,  $300 \leq m/z \leq 400$  and  $m/z > 400$  (Fig. 2b). The molecular weight  
256 distribution of products shifted with the addition of alkaline species. In the experiment without alkaline  
257 species (Exp.IN.1), molecules with high molecular weight ( $m/z > 400$ ) had the highest proportion. In  
258 contrast, DMA reduced the proportion of high molecular weight molecules ( $m/z > 400$ ), while  
259 increasing the intensity of molecules with  $m/z$  values in the ranges  $m/z < 300$  and  $300 \leq m/z \leq 400$   
260 (Exp.IND.1) as shown in Fig. 2b. This suggests that the presence of DMA facilitates the formation of  
261 organic chlorinated compounds with lower molecular weight, which can be attributed to the stronger  
262 neutralization of the acidity by DMA, thereby inhibiting the acid-catalyzed polymerization reaction to  
263 generate high molecular weight molecules (Du et al., 2023). The lower proportion of organic  
264 chlorinated oligomers produced in Exp.IND.1 further supports this speculation (Fig. S4).



265

266 **Figure 2. (a) Total signal intensity of identified organic chlorinated compounds for different experiments. (b)**  
 267 **Distribution of identified molecules under different experimental conditions.**

268 The Van Krevelen (VK) diagrams based on O/C and H/C ratios are presented in Fig. 3a-3b. The H/C  
 269 and O/C ratios of organic chlorinated compounds are primarily distributed in the ranges of 0.9-2.0 and  
 270 0.1-1.0. As shown in Fig. 3c, the organic chlorinated compounds produced in the presence of NH<sub>3</sub>  
 271 (Exp.INA.1) exhibited the highest O/C ratio, which can be attributed to the presence of more hydroxyl,  
 272 carbonyl, and carboxyl functional groups. The OS<sub>C</sub> of organic chlorinated compounds in Exp.INA.1  
 273 was also higher, indicating that NH<sub>3</sub> enhances the degree of oxidation of organic chlorinated  
 274 compounds (Fig. 3d). Conversely, the O/C ratio and OS<sub>C</sub> of organic chlorinated compounds were low  
 275 in the presence of DMA (Exp.IDA.1). Fig. S5 shows that the proportion of dichlorinated compounds in  
 276 the presence of DMA is lower than that in the presence of NH<sub>3</sub>, indicating that less active chlorine was  
 277 produced in the presence of DMA and its multi-generation oxidation was inhibited. This result further  
 278 supports that the weakening effect of DMA on chloride depletion is significantly more effective than  
 279 that of NH<sub>3</sub> as mentioned above. Some organic chlorinated compounds (e.g., C<sub>5</sub>H<sub>7</sub>ClO<sub>4</sub>, C<sub>8</sub>H<sub>11</sub>ClO<sub>5</sub>,  
 280 and C<sub>8</sub>H<sub>13</sub>ClO<sub>6</sub>) detected in this study have also been reported in field observations (Chen et al., 2023),  
 281 indicating that chloride depletion could be a source thereof in the ambient environment. These  
 282 compounds were identified in our previous study and their formation pathways were proposed (Song et  
 283 al., 2026).



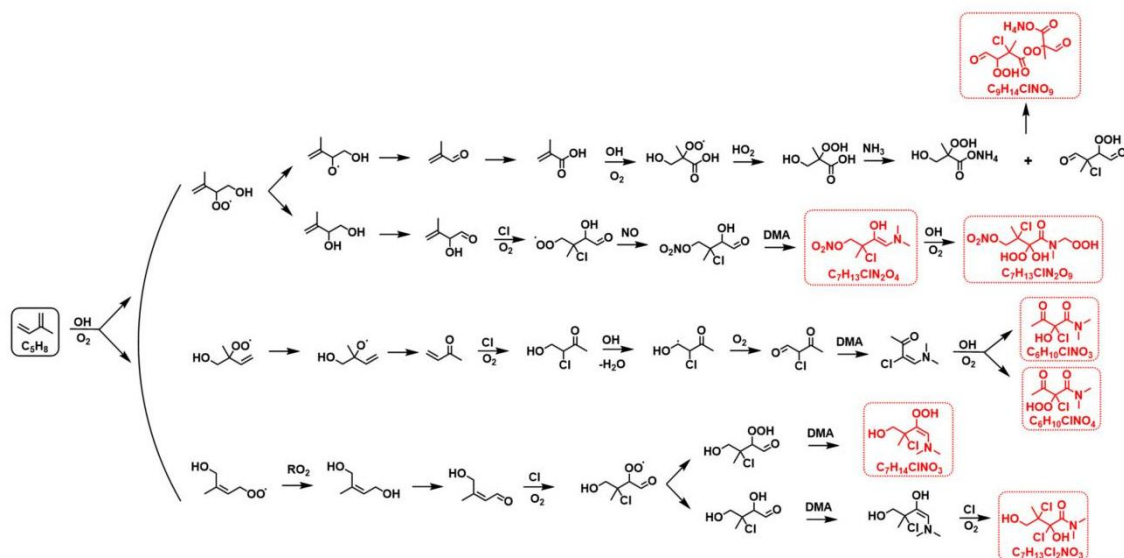
284

285 **Figure 3. Van Krevelen diagram of organic chlorinated compounds for different experiments with NO<sub>x</sub> in the**  
 286 **(a) positive and (b) negative ion modes. The circle size represents the proportion of organic chlorinated**  
 287 **compounds. (c) OS<sub>c</sub> and (d) DBE of organic chlorinated compounds for different experiments with NO<sub>x</sub>. (e)**  
 288 **Fractional contribution to the total unique molecules by CHCINO and CHCIO compounds in the presence of**  
 289 **alkaline species. (f) Nitrogen atom distribution of CHCINO compounds in the presence of alkaline species for**  
 290 **different experiments with NO<sub>x</sub>.**

291 As shown in Fig. S6, many unique molecules were detected in the experiments with alkaline species  
 292 (Exp.INA.1 and Exp.IND.1), in addition to some compounds also detected in Exp.IN.1. In the  
 293 experiment in the presence of NH<sub>3</sub> (Exp.INA.1), 42 and 30 unique molecules were detected in the  
 294 positive and negative ion modes, respectively. When DMA was present (Exp.IDA.1), 45 and 25 unique  
 295 organic chlorinated compounds were identified in the positive and negative modes, respectively. These  
 296 findings suggest that alkaline species alter the molecular composition of organic chlorinated

297 compounds. The identified chlorinated species predominantly consisted of CHClO and CHClNO  
298 compounds, with the proportion of CHClNO being higher than that of CHClO (Fig. 3e). The CHClNO  
299 compounds primarily consist of N<sub>2</sub> products (Fig. 3f), and their formation is favored by high humidity  
300 (Yang et al., 2025). Representative CHClNO compounds include C<sub>9</sub>H<sub>14</sub>ClNO<sub>9</sub>, C<sub>7</sub>H<sub>13</sub>ClN<sub>2</sub>O<sub>4</sub>,  
301 C<sub>6</sub>H<sub>10</sub>ClNO<sub>3</sub>, etc. Fig. 4 presents the formation mechanism of these compounds. Specifically, isoprene  
302 is oxidized by OH radicals to form key intermediates, which can be further oxidized by Cl radicals,  
303 yielding organic chlorinated monomers (e.g., C<sub>4</sub>H<sub>5</sub>ClO<sub>2</sub>, C<sub>5</sub>H<sub>9</sub>ClO<sub>3</sub>, C<sub>5</sub>H<sub>9</sub>ClO<sub>4</sub>). These monomers can  
304 be converted into organic chlorinated oligomers through dehydration reactions or acid-catalyzed  
305 accretion reactions. Notably, NH<sub>3</sub> and DMA can react with these organic chlorinated compounds  
306 through acid-base neutralization to produce CHClNO compounds. For instance, NH<sub>3</sub> can react with  
307 C<sub>4</sub>H<sub>8</sub>O<sub>5</sub> to form C<sub>4</sub>H<sub>11</sub>NO<sub>5</sub>. C<sub>4</sub>H<sub>11</sub>NO<sub>5</sub> and C<sub>5</sub>H<sub>7</sub>ClO<sub>4</sub> can undergo an accretion reaction to form  
308 C<sub>9</sub>H<sub>14</sub>ClNO<sub>9</sub>. In addition, DMA can react with the aldehyde function of organic chlorinated compounds  
309 to form carbinolamines, which then dehydrate to form enamine compounds (e.g., C<sub>7</sub>H<sub>13</sub>ClN<sub>2</sub>O<sub>4</sub> and  
310 C<sub>7</sub>H<sub>14</sub>ClNO<sub>2</sub>). These enamine compounds can be further oxidized by OH and Cl radicals to produce the  
311 observed CHClNO compounds (e.g., C<sub>6</sub>H<sub>10</sub>ClNO<sub>3</sub>, C<sub>7</sub>H<sub>13</sub>Cl<sub>2</sub>NO<sub>3</sub>, C<sub>7</sub>H<sub>13</sub>ClN<sub>2</sub>O<sub>9</sub>).

312 The toxicity prediction results of these organic chlorinated compounds are presented in Table S2.  
313 Results show that C<sub>7</sub>H<sub>13</sub>ClN<sub>2</sub>O<sub>4</sub> compounds have the highest pLD<sub>50</sub> values and are classified as class 3,  
314 indicating that they have considerable potential for acute toxicity. Notably, the predicted developmental  
315 toxicity values for the compounds listed in Table S2 have been classified as the highest hazard level,  
316 and they also pose mutagenicity risks. This highlights the necessity to conduct in-depth research on the  
317 toxicity of organic chlorinated compounds in the coastal atmosphere.

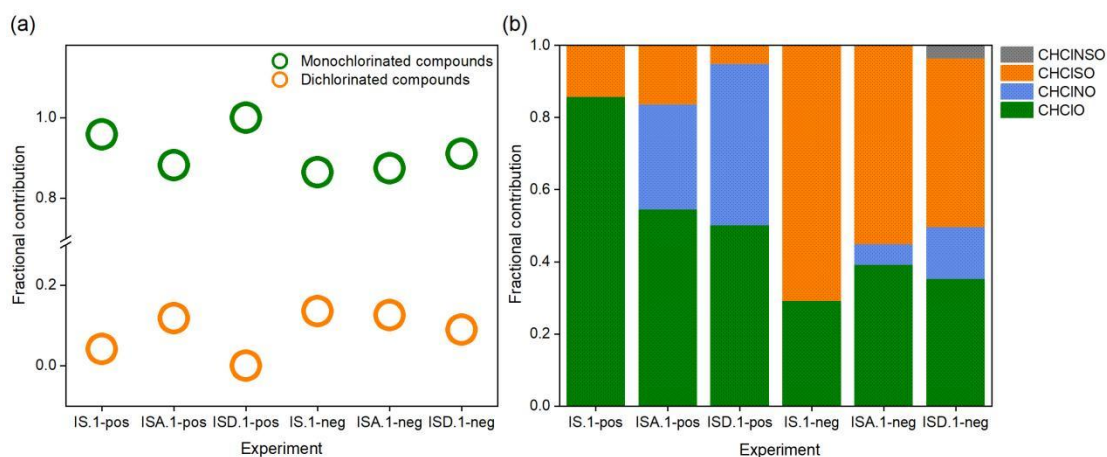


318

319 **Figure 4. (a) Formation mechanism of representative CHCINO compounds. The red boxes indicate the**  
 320 **detected CHCINO compounds in our experiments.**

### 321 3.3.2 Effects of alkaline species in the presence of SO<sub>2</sub>

322 In the presence of SO<sub>2</sub>, the addition of NH<sub>3</sub> and DMA both significantly reduced the abundance of high  
 323 molecular weight compounds (Fig. S7) and the total signal intensity of organic chlorinated compounds  
 324 (Fig. 5a), which can be attributed to a reduced activation of chloride ions. This might be due to the fact  
 325 that the addition of alkaline species reduces the production of gaseous HCl as a result of acid-base  
 326 neutralization reactions and further diminishes the source of active chlorine (Edwards et al., 2024;  
 327 Song et al., 2025). In addition, chloride ions can be activated into active chlorine by strong oxidants  
 328 (OH radicals, O<sub>3</sub>, etc.) (Zhang and Chan, 2023; Su et al., 2022). DMA can compete with chloride ions  
 329 for these oxidants, thereby limiting the activation of chloride ions and reducing the generation of active  
 330 chlorine species (Møller et al., 2020). The proportion of dichlorinated compounds in Exp.ISD.1 was  
 331 significantly lower than that in Exp.IS.1 (Fig. 5a), mainly due to the reduction of active chlorine that  
 332 inhibited its multi-generation oxidation. This further explains that the weakening effect of DMA on  
 333 chloride depletion is enhanced in the presence of isoprene and SO<sub>2</sub>.



334

335 **Figure 5. (a) Fractional contribution of monochlorinated and dichlorinated compounds in the total organic**  
 336 **chlorinated compounds for different experiments with SO<sub>2</sub>. (b) Fractional contribution to the total organic**  
 337 **chlorinated compounds by different compounds.**

338 As shown in Fig. 5b, in experiments with SO<sub>2</sub>, the products detected in the positive ion mode mainly  
 339 consisted of CHCLO compounds, while the proportion of CHCISO compounds was the highest in the  
 340 negative ion mode. This may be related to the different sensitivities of the compounds in different ion  
 341 modes. CHCINO and CHCINSO compounds (including C<sub>7</sub>H<sub>15</sub>CIN<sub>2</sub>O<sub>6</sub>, C<sub>13</sub>H<sub>19</sub>CIN<sub>2</sub>O<sub>6</sub>, C<sub>18</sub>H<sub>35</sub>CIN<sub>2</sub>SO<sub>8</sub>,  
 342 etc.) were also detected in experiments in the presence of alkaline species and SO<sub>2</sub>. As mentioned  
 343 above, the CHCINO compounds can be formed through the acid-base neutralization reaction or the  
 344 reaction of DMA with aldehyde function. These compounds can react with H<sub>2</sub>SO<sub>4</sub> through  
 345 esterification reactions to form CHCINSO compounds. The observed higher proportion of CHCINO  
 346 compounds in Exp.ISD.1 than that in Exp.ISA.1 (Fig. 5b) may result from the stronger ability of DMA  
 347 to react with organic acids or carbonyl compounds (Smith et al., 2021). Moreover, autoxidation via a  
 348 unimolecular reaction, being an important oxidation pathway for DMA in the atmosphere, facilitates  
 349 the formation of hydroperoxy amides (Møller et al., 2020). Overall, alkaline gases affect the formation  
 350 of active chlorine during chloride depletion, and alters the composition of organic chlorinated  
 351 compounds.

#### 352 4. Conclusions

353 The complexity of atmospheric pollutants in coastal environments hinders the understanding of the  
 354 mechanisms influencing chloride depletion. This study explored the detailed effects of NH<sub>3</sub> and DMA  
 355 on this phenomenon. The results demonstrated that NH<sub>3</sub> and DMA could weaken the chloride depletion  
 356 induced by acidic gases, with DMA exhibiting a more substantial weakening effect than NH<sub>3</sub>. This

357 difference in their impact is primarily due to DMA's stronger alkalinity and nucleation ability, which  
358 enable it to interact more effectively with acidic species than NH<sub>3</sub>. Although the concentration of DMA  
359 in the atmosphere is lower than that of NH<sub>3</sub>, its impact on chloride depletion is essential. The current  
360 results further reveal that considering only the effects of acidic gases may lead to deviations in the  
361 prediction of chloride depletion. This underscores the necessity to examine the role of alkaline species,  
362 especially organic amines, in future field studies of chloride depletion.

363 The mass spectrometry results showed that the presence of alkaline species also reduces the formation  
364 of organic chlorinated compounds, indicating that the generation of active chlorine is inhibited during  
365 chloride depletion. This can be attributed to the fact that the alkaline species reduce the generation of  
366 gaseous HCl through acid-base neutralization reactions, and can compete with chloride ions for  
367 oxidants, thereby further reducing the production of active chlorine. This further supports the idea that  
368 alkaline species could weaken the chloride depletion process. Additionally, the presence of alkaline  
369 species, especially DMA, promotes the formation of low-molecular-weight organic chlorinated  
370 compounds by neutralizing acidity, thereby inhibiting acid-catalyzed polymerization and the formation  
371 of high-molecular-weight compounds. The addition of alkaline species was observed to alter the  
372 composition of organic chlorinated compounds, with several identified unique products that were not  
373 present under acidic conditions. This suggests that alkaline species not only inhibit chloride depletion  
374 but also influence the overall chemical composition of the atmosphere by altering the chlorination  
375 pathways of organic compounds. The current results strengthen our understanding of the mechanism  
376 influencing chloride depletion, and provide a ground for the future identification of organic chlorinated  
377 compounds in ambient samples.

378 The initial concentrations of alkaline species used in the experiments were higher than the ambient  
379 levels. Moreover, the complex atmospheric chemical reactions were simplified in this study to  
380 eliminate the interference from other factors. Future studies should consider evaluating the effects of  
381 composition and phase state of aerosols on the mechanism and the extent of chloride depletion.

#### 382 **Data availability**

383 Experimental data can be found at <https://doi.org/10.5281/zenodo.18795123>.

384 **Supplement**

385 The supplement related to this article is available online at:

386 **Author contributions**

387 LD and AS designed the experiments, and AS carried them out. AS performed data analysis with  
388 assistance from LD, KL, and LX. AS wrote the paper with contributions from all co-authors, and  
389 co-authors commented on the paper.

390 **Competing interest**

391 The contact author has declared that none of the authors has any competing interests.

392 **Acknowledgements**

393 We thank Guannan Lin from the State Key Laboratory of Microbial Technology of Shandong  
394 University for help and guidance with UPLC/ESI-HR-Q-TOF-MS measurements.

395 **Financial support**

396 This work was supported by National Key Research and Development Program of China  
397 (2023YFC3706203), National Natural Science Foundation of China (U25A20787, 22376121), and  
398 Intramural Joint Program Fund of State Key Laboratory of Microbial Technology  
399 (SKLMTIJP-2025-02).

400 **References**

401 Armstrong, N. C., Chen, Y., Cui, T., Zhang, Y., Christensen, C., Zhang, Z., Turpin, B. J., Chan, M. N.,  
402 Gold, A., Ault, A. P., and Surratt, J. D.: Isoprene epoxydiol-derived sulfated and nonsulfated oligomers  
403 suppress particulate mass loss during oxidative aging of secondary organic aerosol, *Environ. Sci.*  
404 *Technol.*, 56, 16611-16620, <https://doi.org/10.1021/acs.est.2c03200>, 2022.  
405 Bates, K. H., Jacob, D. J., Cope, J. D., Chen, X., Millet, D. B., and Nguyen, T. B.: Emerging  
406 investigator series: Aqueous oxidation of isoprene-derived organic aerosol species as a source of

407 atmospheric formic and acetic acids, *Environ. Sci.: Atmos.*, 3, 1651-1664,  
408 <https://doi.org/10.1039/d3ea00076a>, 2023.

409 Behera, S. N. and Sharma, M.: Degradation of SO<sub>2</sub>, NO<sub>2</sub> and NH<sub>3</sub> leading to formation of secondary  
410 inorganic aerosols: An environmental chamber study, *Atmos. Environ.*, 45, 4015-4024,  
411 <https://doi.org/10.1016/j.atmosenv.2011.04.056>, 2011.

412 Behera, S. N. and Sharma, M.: Transformation of atmospheric ammonia and acid gases into  
413 components of PM<sub>2.5</sub>: An environmental chamber study, *Environ Sci Pollut Res* 19, 1187-1197,  
414 <https://doi.org/10.1007/s11356-011-0635-9>, 2012.

415 Behera, S. N., Sharma, M., Aneja, V. P., and Balasubramanian, R.: Ammonia in the atmosphere: A  
416 review on emission sources, atmospheric chemistry and deposition on terrestrial bodies, *Environ Sci*  
417 *Pollut Res*, 20, 8092-8131, <https://doi.org/10.1007/s11356-013-2051-9>, 2013.

418 Berner, A. H. and David Felix, J.: Investigating ammonia emissions in a coastal urban airshed using  
419 stable isotope techniques, *Sci. Total Environ.*, 707, 134952,  
420 <https://doi.org/10.1016/j.scitotenv.2019.134952>, 2020.

421 Bian, Q., Huang, X. H. H., and Yu, J. Z.: One-year observations of size distribution characteristics of  
422 major aerosol constituents at a coastal receptor site in Hong Kong – Part 1: Inorganic ions and oxalate,  
423 *Atmos. Chem. Phys.*, 14, 9013-9027, <https://doi.org/10.5194/acp-14-9013-2014>, 2014.

424 Braun, R. A., Dadashazar, H., MacDonald, A. B., Aldhaif, A. M., Maudlin, L. C., Crosbie, E., Aghdam,  
425 M. A., Hossein Mardi, A., and Sorooshian, A.: Impact of wildfire emissions on chloride and bromide  
426 depletion in marine aerosol particles, *Environ. Sci. Technol.*, 51, 9013-9021,  
427 <https://doi.org/10.1021/acs.est.7b02039>, 2017.

428 Chen, D.-P., Ma, W., Yang, C.-H., Li, M., Zhou, Z.-Z., Zhang, Y., Wang, X.-C., and Quan, Z.-J.:  
429 Formation of atmospheric molecular clusters containing nitric acid with ammonia, methylamine, and  
430 dimethylamine, *Environ. Sci.: Processes Impacts*, 26, 2036-2050, <https://doi.org/10.1039/d4em00330f>,  
431 2024a.

432 Chen, D., Yao, X., Chan, C. K., Tian, X., Chu, Y., Clegg, S. L., Shen, Y., Gao, Y., and Gao, H.:  
433 Competitive uptake of dimethylamine and trimethylamine against ammonia on acidic particles in  
434 marine atmospheres, *Environ. Sci. Technol.*, 56, 5430-5439, <https://doi.org/10.1021/acs.est.1c08713>,  
435 2022.

436 Chen, G., Xu, L., Yu, S., Xue, L., Lin, Z., Yang, C., Ji, X., Fan, X., Tham, Y. J., Wang, H., Hong, Y., Li,

437 M., Seinfeld, J. H., and Chen, J.: Increasing contribution of chlorine chemistry to wintertime ozone  
438 formation promoted by enhanced nitrogen chemistry, *Environ. Sci. Technol.*, 58, 22714-22721,  
439 <https://doi.org/10.1021/acs.est.4c09523>, 2024b.

440 Chen, H., Yan, C., Fu, Q., Wang, X., Tang, J., Jiang, B., Sun, H., Luan, T., Yang, Q., Zhao, Q., Li, J.,  
441 Zhang, G., Zheng, M., Zhou, X., Chen, B., Du, L., Zhou, R., Zhou, T., and Xue, L.: Optical properties  
442 and molecular composition of wintertime atmospheric water-soluble organic carbon in different coastal  
443 cities of eastern China, *Sci. Total Environ.*, 892, 164702,  
444 <https://doi.org/10.1016/j.scitotenv.2023.164702>, 2023.

445 Chen, W., Wang, X., Cohen, J. B., Zhou, S., Zhang, Z., Chang, M., and Chan, C.-Y.: Properties of  
446 aerosols and formation mechanisms over southern China during the monsoon season, *Atmos. Chem.*  
447 *Phys.*, 16, 13271-13289, <https://doi.org/10.5194/acp-16-13271-2016>, 2016.

448 Dai, J., Wang, T., Shen, H., Xia, M., Sun, W., and Brasseur, G. P.: Significant impact of a daytime  
449 halogen oxidant on coastal air quality, *Environ. Sci. Technol.*, 59, 2169-2180,  
450 <https://doi.org/10.1021/acs.est.4c08360>, 2025.

451 DeRieux, W.-S. W., Lakey, P. S. J., Chu, Y., Chan, C. K., Glicker, H. S., Smith, J. N., Zuend, A., and  
452 Shiraiwa, M.: Effects of phase state and phase separation on dimethylamine uptake of ammonium  
453 sulfate and ammonium sulfate–sucrose mixed particles, *ACS Earth Space Chem.*, 3, 1268-1278,  
454 <https://doi.org/10.1021/acsearthspacechem.9b00142>, 2019.

455 DeRieux, W.-S. W., Li, Y., Lin, P., Laskin, J., Laskin, A., Bertram, A. K., Nizkorodov, S. A., and  
456 Shiraiwa, M.: Predicting the glass transition temperature and viscosity of secondary organic material  
457 using molecular composition, *Atmos. Chem. Phys.*, 18, 6331-6351,  
458 <https://doi.org/10.5194/acp-18-6331-2018>, 2018.

459 Du, L., Xu, L., Li, K., George, C., and Ge, M.: NH<sub>3</sub> weakens the enhancing effect of SO<sub>2</sub> on biogenic  
460 secondary organic aerosol formation, *Environ. Sci. Technol. Lett.*, 10, 145-151,  
461 <https://doi.org/10.1021/acs.estlett.2c00959>, 2023.

462 Du, W., Wang, X., Yang, F., Bai, K., Wu, C., Liu, S., Wang, F., Lv, S., Chen, Y., Wang, J., Liu, W.,  
463 Wang, L., Chen, X., and Wang, G.: Particulate amines in the background atmosphere of the Yangtze  
464 River Delta, China: Concentration, size distribution, and sources, *Adv. Atmos. Sci.*, 38, 1128-1140,  
465 <https://doi.org/10.1007/s00376-021-0274-0>, 2021.

466 Duan, Y., Liu, Y., Zhang, K., Li, L., Huo, J., Chen, J., Fu, Q., Gao, Z., Xiu, G., and Hu, T.: Variations of

467 chloride depletion and its impacts on ozone formation: Case study of a coastal area in Shanghai, *Sci.*  
468 *Total Environ.*, 957, 176899, <https://doi.org/10.1016/j.scitotenv.2024.176899>, 2024.

469 Edwards, E.-L., Choi, Y., Crosbie, E. C., DiGangi, J. P., Diskin, G. S., Robinson, C. E., Shook, M. A.,  
470 Winstead, E. L., Ziemba, L. D., and Sorooshian, A.: Sea salt reactivity over the northwest Atlantic: An  
471 in-depth look using the airborne ACTIVATE dataset, *Atmos. Chem. Phys.*, 24, 3349-3378,  
472 <https://doi.org/10.5194/acp-24-3349-2024>, 2024.

473 Ghosh, A., Roy, A., Das, S. K., Ghosh, S. K., Raha, S., and Chatterjee, A.: Identification of most  
474 preferable reaction pathways for chloride depletion from size segregated sea-salt aerosols: A study over  
475 high altitude Himalaya, tropical urban metropolis and tropical coastal mangrove forest in eastern India,  
476 *Chemosphere*, 245, 125673, <https://doi.org/10.1016/j.chemosphere.2019.125673>, 2020.

477 Hoffmann, E. H., Tilgner, A., Wolke, R., and Herrmann, H.: Enhanced chlorine and bromine atom  
478 activation by hydrolysis of halogen nitrates from marine aerosols at polluted coastal areas, *Environ. Sci.*  
479 *Technol.*, 53, 771-778, <https://doi.org/10.1021/acs.est.8b05165>, 2019.

480 Jenkin, M. E., Young, J. C., and Rickard, A. R.: The MCM v3.3.1 degradation scheme for isoprene,  
481 *Atmos. Chem. Phys.*, 15, 11433-11459, <https://doi.org/10.5194/acp-15-11433-2015>, 2015.

482 Kupiainen, O., Ortega, I. K., Kurtén, T., and Vehkamäki, H.: Amine substitution into sulfuric acid –  
483 ammonia clusters, *Atmos. Chem. Phys.*, 12, 3591-3599, <https://doi.org/10.5194/acp-12-3591-2012>,  
484 2012.

485 Lan, Z., Lin, W., and Zhao, G.: Sources, variations, and effects on air quality of atmospheric ammonia,  
486 *Curr Pollution Rep*, 10, 40-53, <https://doi.org/10.1007/s40726-023-00291-6>, 2024.

487 Li, X., Jia, L., Xu, Y., and Pan, Y.: A novel reaction between ammonia and Criegee intermediates can  
488 form amines and suppress oligomers from isoprene, *Sci. Total Environ.*, 956, 177389,  
489 <https://doi.org/10.1016/j.scitotenv.2024.177389>, 2024.

490 Liu, M., Wang, X., Liu, Z., Jiang, Y., Li, M., Zhang, J., Sun, Y., Zhu, Y., Xue, L., and Wang, W.:  
491 Characteristics and origins of fine particulate amines at a coastal mountain site in northern China in  
492 spring, *Atmos. Environ.*, 321, <https://doi.org/10.1016/j.atmosenv.2024.120365>, 2024a.

493 Liu, M., Wang, X., Liu, Z., Jiang, Y., Li, M., Zhang, J., Sun, Y., Zhu, Y., Xue, L., and Wang, W.:  
494 Characteristics and origins of fine particulate amines at a coastal mountain site in northern China in  
495 spring, *Atmos. Environ.*, 321, 120365, <https://doi.org/10.1016/j.atmosenv.2024.120365>, 2024b.

496 Liu, T., Xu, Y., Sun, Q. B., Xiao, H. W., Zhu, R. G., Li, C. X., Li, Z. Y., Zhang, K. Q., Sun, C. X., and

497 Xiao, H. Y.: Characteristics, origins, and atmospheric processes of amines in fine aerosol particles in  
498 winter in China, *J. Geophys. Res. Atmos.*, 128, e2023JD038974, <https://doi.org/10.1029/2023jd038974>,  
499 2023.

500 Liu, X., Liu, L., Zhang, B., Liu, P., Huang, R.-J., Hildebrandt Ruiz, L., Miao, R., Chen, Q., and Wang,  
501 X.: Modeling the global impact of chlorine chemistry on secondary organic aerosols, *Environ. Sci.*  
502 *Technol.*, 58, 23064-23074, <https://doi.org/10.1021/acs.est.4c05037>, 2024c.

503 Liu, Z., Li, M., Wang, X., Liang, Y., Jiang, Y., Chen, J., Mu, J., Zhu, Y., Meng, H., Yang, L., Hou, K.,  
504 Wang, Y., and Xue, L.: Large contributions of anthropogenic sources to amines in fine particles at a  
505 coastal area in northern China in winter, *Sci. Total Environ.*, 839, 156281,  
506 <https://doi.org/10.1016/j.scitotenv.2022.156281>, 2022.

507 Loukonen, V., Kurtén, T., Ortega, I. K., Vehkamäki, H., Pádua, A. A. H., Sellegri, K., and Kulmala, M.:  
508 Enhancing effect of dimethylamine in sulfuric acid nucleation in the presence of water – a  
509 computational study, *Atmos. Chem. Phys.*, 10, 4961-4974, <https://doi.org/10.5194/acp-10-4961-2010>,  
510 2010.

511 Lu, Y., Liu, L., Ning, A., Yang, G., Liu, Y., Kurtén, T., Vehkamäki, H., Zhang, X., and Wang, L.:  
512 Atmospheric sulfuric acid-dimethylamine nucleation enhanced by trifluoroacetic acid, *Geophys. Res.*  
513 *Lett.*, 47, e2019GL085627, <https://doi.org/10.1029/2019gl085627>, 2020.

514 Møller, K. H., Berndt, T., and Kjaergaard, H. G.: Atmospheric autoxidation of amines, *Environ. Sci.*  
515 *Technol.*, 54, 11087-11099, <https://doi.org/10.1021/acs.est.0c03937>, 2020.

516 Murphy, S. M., Sorooshian, A., Kroll, J. H., Ng, N. L., Chhabra, P., Tong, C., Surratt, J. D., Knipping,  
517 E., Flagan, R. C., and Seinfeld, J. H.: Secondary aerosol formation from atmospheric reactions of  
518 aliphatic amines, *Atmos. Chem. Phys.*, 7, 2313–2337, <https://doi.org/10.5194/acp-7-2313-2007>, 2007.

519 Nielsen, C. J., Herrmann, H., and Weller, C.: Atmospheric chemistry and environmental impact of the  
520 use of amines in carbon capture and storage (CCS), *Chem. Soc. Rev.*, 41, 6684–6704,  
521 <https://doi.org/10.1039/c2cs35059a>, 2012.

522 Nolte, C., Bhave, P., Arnold, J., Dennis, R., Zhang, K., and Wexler, A.: Modeling urban and regional  
523 aerosols—Application of the CMAQ-UCD aerosol model to Tampa, a coastal urban site, *Atmos.*  
524 *Environ.*, 42, 3179-3191, <https://doi.org/10.1016/j.atmosenv.2007.12.059>, 2008.

525 Nolte, C. G., Appel, K. W., Kelly, J. T., Bhave, P. V., Fahey, K. M., Collett Jr., J. L., Zhang, L., and  
526 Young, J. O.: Evaluation of the Community Multiscale Air Quality (CMAQ) model v5.0 against

527 size-resolved measurements of inorganic particle composition across sites in North America, *Geosci.*  
528 *Model Dev.*, 8, 2877-2892, <https://doi.org/10.5194/gmd-8-2877-2015>, 2015.

529 Ortega, I. K., Kupiainen, O., Kurtén, T., Olenius, T., Wilkman, O., McGrath, M. J., Loukonen, V., and  
530 Vehkamäki, H.: From quantum chemical formation free energies to evaporation rates, *Atmos. Chem.*  
531 *Phys.*, 12, 225-235, <https://doi.org/10.5194/acp-12-225-2012>, 2012.

532 Rankin, A. M. and Wolff, E. W.: A year-long record of size-segregated aerosol composition at Halley,  
533 Antarctica, *J. Geophys. Res. Atmos.*, 108, 4775, <https://doi.org/10.1029/2003jd003993>, 2003.

534 Sauerwein, M. and Chan, C. K.: Heterogeneous uptake of ammonia and dimethylamine into sulfuric  
535 and oxalic acid particles, *Atmos. Chem. Phys.*, 17, 6323-6339,  
536 <https://doi.org/10.5194/acp-17-6323-2017>, 2017.

537 Smith, A. M., Keene, W. C., Maben, J. R., Pszenny, A. A. P., Fischer, E., and Stohl, A.: Ammonia  
538 sources, transport, transformation, and deposition in coastal New England during summer, *J. Geophys.*  
539 *Res. Atmos.*, 112, <https://doi.org/10.1029/2006jd007574>, 2007.

540 Smith, N. R., Montoya-Aguilera, J., Dabdub, D., and Nizkorodov, S. A.: Effect of humidity on the  
541 reactive uptake of ammonia and dimethylamine by nitrogen-containing secondary organic aerosol,  
542 *Atmosphere*, 12, <https://doi.org/10.3390/atmos12111502>, 2021.

543 Song, A., Li, K., Yang, Z., Tsona Tchinda, N., and Du, L.: Marine volatile organic compounds promote  
544 the chloride depletion in sea salt aerosols, *J. Geophys. Res. Atmos.*, 130, e2025JD043495,  
545 <https://doi.org/10.1029/2025JD043495>, 2025.

546 Song, A., Li, K., Yang, Z., Xu, L., Chen, X., Tsona Tchinda, N., and Du, L.: Anthropogenic-Biogenic  
547 interaction drives chloride depletion in coastal atmospheres, under review, 2026.

548 Su, B., Wang, T., Zhang, G., Liang, Y., Lv, C., Hu, Y., Li, L., Zhou, Z., Wang, X., and Bi, X.: A review  
549 of atmospheric aging of sea spray aerosols: Potential factors affecting chloride depletion, *Atmos.*  
550 *Environ.*, 290, 119365, <https://doi.org/10.1016/j.atmosenv.2022.119365>, 2022.

551 Wach, P., Spólnik, G., Surratt, J. D., Blaziak, K., Rudzinski, K. J., Lin, Y.-H., Maenhaut, W.,  
552 Danikiewicz, W., Claeys, M., and Szmigielski, R.: Structural characterization of lactone-containing  
553 MW 212 organosulfates originating from isoprene oxidation in ambient fine aerosol, *Environ. Sci.*  
554 *Technol.*, 54, 1415-1424, <https://doi.org/10.1021/acs.est.9b06190>, 2020.

555 Wang, C., Liu, Y., Huang, T., Feng, Y., Wang, Z., Lu, R., and Jiang, S.: Sulfuric acid–dimethylamine  
556 particle formation enhanced by functional organic acids: An integrated experimental and theoretical

557 study, *Phys. Chem. Chem. Phys.*, 24, 23540-23550, <https://doi.org/10.1039/d2cp01671k>, 2022a.

558 Wang, D. S., Masoud, C. G., Modi, M., and Hildebrandt Ruiz, L.: Isoprene–chlorine oxidation in the  
559 presence of NO<sub>x</sub> and implications for urban atmospheric chemistry, *Environ. Sci. Technol.*, 56,  
560 9251-9264, <https://doi.org/10.1021/acs.est.1c07048>, 2022b.

561 Wang, L., Lal, V., Khalizov, A. F., and Zhang, R.: Heterogeneous chemistry of alkylamines with  
562 sulfuric acid implications for atmospheric formation-of alkylammonium sulfates, *Environ. Sci. Technol.* ,  
563 44, 2461–2465, <https://doi.org/10.1021/es9036868>, 2010.

564 Wang, M., Kong, W., Marten, R., He, X.-C., Chen, D., Pfeifer, J., Heitto, A., Kontkanen, J., Dada, L.,  
565 Kürten, A., Yli-Juuti, T., Manninen, H. E., Amanatidis, S., Amorim, A., Baalbaki, R., Baccarini, A.,  
566 Bell, D. M., Bertozzi, B., Bräkling, S., Brilke, S., Murillo, L. C., Chiu, R., Chu, B., De Menezes, L.-P.,  
567 Duplissy, J., Finkenzeller, H., Carracedo, L. G., Granzin, M., Guida, R., Hansel, A., Hofbauer, V.,  
568 Krechmer, J., Lehtipalo, K., Lamkaddam, H., Lampimäki, M., Lee, C. P., Makhmutov, V., Marie, G.,  
569 Mathot, S., Mauldin, R. L., Mentler, B., Müller, T., Onnela, A., Partoll, E., Petäjä, T., Philippov, M.,  
570 Pospisilova, V., Ranjithkumar, A., Rissanen, M., Rörup, B., Scholz, W., Shen, J., Simon, M., Sipilä, M.,  
571 Steiner, G., Stolzenburg, D., Tham, Y. J., Tomé, A., Wagner, A. C., Wang, D. S., Wang, Y., Weber, S. K.,  
572 Winkler, P. M., Wlasits, P. J., Wu, Y., Xiao, M., Ye, Q., Zauner-Wieczorek, M., Zhou, X., Volkamer, R.,  
573 Riipinen, I., Dommen, J., Curtius, J., Baltensperger, U., Kulmala, M., Worsnop, D. R., Kirkby, J.,  
574 Seinfeld, J. H., El-Haddad, I., Flagan, R. C., and Donahue, N. M.: Rapid growth of new atmospheric  
575 particles by nitric acid and ammonia condensation, *Nature*, 581, 184-189,  
576 <https://doi.org/10.1038/s41586-020-2270-4>, 2020.

577 Wennberg, P. O., Bates, K. H., Crouse, J. D., Dodson, L. G., McVay, R. C., Mertens, L. A., Nguyen, T.  
578 B., Praske, E., Schwantes, R. H., Smarte, M. D., St Clair, J. M., Teng, A. P., Zhang, X., and Seinfeld, J.  
579 H.: Gas-phase reactions of isoprene and its major oxidation products, *Chem. Rev.*, 118, 3337-3390,  
580 <https://doi.org/10.1021/acs.chemrev.7b00439>, 2018.

581 Wolfe, G. M., Marvin, M. R., Roberts, S. J., Travis, K. R., and Liao, J.: The Framework for 0-D  
582 Atmospheric Modeling (F0AM) v3.1, *Geosci. Model Dev.*, 9, 3309-3319,  
583 <https://doi.org/10.5194/gmd-9-3309-2016>, 2016.

584 Wu, K., Zhu, S., Liu, Y., Wang, H., Yang, X., Liu, L., Dabdub, D., and Cappa, C. D.: Modeling  
585 ammonia and its uptake by secondary organic aerosol over China, *J. Geophys. Res. Atmos.*, 126,  
586 e2020JD034109, <https://doi.org/10.1029/2020jd034109>, 2021.

587 Xie, H., Feng, L., Hu, Q., Zhu, Y., Gao, H., Gao, Y., and Yao, X.: Concentration and size distribution of  
588 water-extracted dimethylammonium and trimethylammonium in atmospheric particles during nine  
589 campaigns - Implications for sources, phase states and formation pathways, *Sci. Total Environ.*,  
590 631-632, 130-141, <https://doi.org/10.1016/j.scitotenv.2018.02.303>, 2018.

591 Xu, L., Liu, X., Gao, H., Yao, X., Zhang, D., Bi, L., Liu, L., Zhang, J., Zhang, Y., Wang, Y., Yuan, Q.,  
592 and Li, W.: Long-range transport of anthropogenic air pollutants into the marine air: Insight into fine  
593 particle transport and chloride depletion on sea salts, *Atmos. Chem. Phys.*, 21, 17715-17726,  
594 <https://doi.org/10.5194/acp-21-17715-2021>, 2021.

595 Yang, Z., Li, K., and Du, L.: Highly oxidized molecules make a significant contribution to enhanced  
596 aromatic-derived secondary organic aerosol under a humid environment, *Adv. Atmos. Sci.*, 42, 641-652,  
597 <https://doi.org/10.1007/s00376-024-4085-y>, 2025.

598 Yao, X., Fang, M., and Chan, C. K.: The size dependence of chloride depletion in fine and coarse  
599 sea-salt particles, *Atmos. Environ.*, 37, 743-751, [https://doi.org/10.1016/S1352-2310\(02\)00955-X](https://doi.org/10.1016/S1352-2310(02)00955-X),  
600 2003.

601 Yu, Z. and Li, Y.: Marine volatile organic compounds and their impacts on marine aerosol—A review,  
602 *Sci. Total Environ.*, 768, 145054, <https://doi.org/10.1016/j.scitotenv.2021.145054>, 2021.

603 Zhan, J., Li, W., Chen, L., Lin, Q., and Gao, Y.: Anthropogenic influences on aerosols at Ny-Ålesund in  
604 the summer Arctic, *Atmos. Pollut. Res.*, 8, 383-393, <https://doi.org/10.1016/j.apr.2016.10.010>, 2017.

605 Zhang, R. and Chan, C. K.: Simultaneous formation of sulfate and nitrate via co-uptake of SO<sub>2</sub> and  
606 NO<sub>2</sub> by aqueous NaCl droplets: Combined effect of nitrate photolysis and chlorine chemistry, *Atmos.*  
607 *Chem. Phys.*, 23, 6113-6126, <https://doi.org/10.5194/acp-23-6113-2023>, 2023.

608 Zhang, W., Ji, Y., Li, G., Shi, Q., and An, T.: The heterogeneous reaction of dimethylamine/ammonia  
609 with sulfuric acid to promote the growth of atmospheric nanoparticles, *Environ. Sci.: Nano*, 6,  
610 2767-2776, <https://doi.org/10.1039/c9en00619b>, 2019.

611 Zhang, W., Weber, J., Archibald, A. T., Abraham, N. L., Booge, D., Yang, M., and Gu, D.: Global  
612 atmospheric composition effects from marine Isoprene emissions, *Environ. Sci. Technol.*, 59,  
613 2554-2564, <https://doi.org/10.1021/acs.est.4c10657>, 2025.

614 Zhou, S., Salter, M., Bertram, T., Brito Azevedo, E., Reis, F., and Wang, J.: Shoreline wave breaking  
615 strongly enhances the coastal sea spray aerosol population: Climate and air quality implications, *Sci.*  
616 *Adv.*, 11, eadw0343, <https://doi.org/10.1126/sciadv.adw0343>, 2025.

617 Zou, Z., Chen, Q., Xia, M., Yuan, Q., Chen, Y., Wang, Y., Xiong, E., Wang, Z., and Wang, T.: OH  
618 measurements in the coastal atmosphere of South China: Possible missing OH sinks in aged air masses,  
619 Atmos. Chem. Phys., 23, 7057-7074, <https://doi.org/10.5194/acp-23-7057-2023>, 2023.

620